International Journal of Basic and Applied Chemical Sciences ISSN: 2277-2073 (Online)
An Open Access, Online International Journal Available at http://www.cibtech.org/jcs.htm
2014 Vol. 4 (2) April-June, pp.36-48/Songca et al.
Research Article

FUNCTIONALIZATION AND CHARACTERIZATION OF PORPHYRIN-CAPPED IRON OXIDE-GOLD CORE-SHELL NANOPARTICLES

***S.P. Songca[1], O.S. Oluwafemi[2], A. Eshilokun[3], A. Strydom[4], R. Tshikhudo[5], S. Debeila[5] and T. Hillie[6]**

[1]Department of Chemistry and Chemical Technology, Faculty of Science, Engineering and Technology, Walter Sisulu University, PO Box 19712, Tecoma, East London, Eastern Cape, South Africa.
[2]Department of Chemistry and Chemical Technology, Walter Sisulu University, 1 Nelson Mandela Drive, Mthatha, Eastern Cape, South Africa.
[3]Department of Chemistry, University of Limpopo, Medunsa Campus, PO Box 135, Medunsa, South Africa, 0204.
[4]Physics Department, University of Johannesburg, C1-Lab 140, PO Box 524, Auckland Park 2006, South Africa.
[5]Advanced Materials Division, Mintek, Private Bag X3015, Randburg, South Africa, 2125.
[6]National Centre for Nano-structured Materials, National Centre for Nano-Structured Materials, CSIR, PO Box 395, Pretoria, 0001.

ABSTRACT

This paper describes the synthesis of Fe_2O_3@Au-NPs, deposition of 5,10,15,20-tetrakis[(3-thioacetoxy-1-propyloxy)phenyl]porphyrin and characterization of the NPs. Fe_2O_3@Au-NPs were synthesized in aqueous solution by overgrowing the gold shell onto Fe_2O_3seeds. Shaking the resulting solution with a dichloromethane solution of the porphyrin leads to transfer of the Fe_2O_3@Au-NPs and deposition of the porphyrin onto the Au surface. TEM showed well dispersed NPs with broad size distribution; d = 34–54 nm (44.26± 6.93), σ = 0.16. AFM confirmed the dispersion observed with TEM. HRTEM showed the core-shell structure and the porphyrin layer. XRD confirmed the presence of Au and Fe. SQUID magnetometry of the porphyrincapped Fe_2O_3@Au-NPs (2-300 K) gave T_B =15.7 ± 0.1 K, negligible hysteresis at room temperature, and significant hysteresis below T_B. Kinetic studies showed rapid transfer of the Fe_2O_3@Au-NPs from the aqueous to the organic phase in the presence of dissolved porphyrin and no such transfer in the absence of dissolved porphyrin, suggesting that the phase transfer of the Fe_2O_3@Au-NPs was followed by binding of the porphyrin to the surface of the NPs in the organic phase. Binding of the porphyrin to the gold surface of the NPs, was also studied with FT-IR.

Keywords: *Photodynamic Therapy, Porphyrin Functionalized Nanoparticles, Core-Shell, Iron Oxide, Gold, SPION*

INTRODUCTION

The technologies of magnetic nanoparticles for biomedical purposes have been developed to such a stage where it is now possible to produce, characterize and specifically tailor the functional properties of the core–shell type of magnetic nanoparticles for clinical applications by functionalizing the external shell with suitable organic and bio-molecules such as porphyrins, phthalocyanines, glycosides, polypeptides and polynucleotides. Nanoparticles comprised of a gold shell and magnetic core such as iron, iron oxide, Cadmium Selenide or Zinc Selenide can be synthesized by overgrowing the gold outer shell onto as synthesized magnetic seed cores (Lu *et al.,* 2006). The magnetic cores of the particles provide the magnetic properties while the gold shell provides a functionalizable surface onto which desired ligands can be chemically bonded, and one that is sufficiently inert not to be biodegraded in the biological media of blood vessels and cell interiors.

Nanoparticles are widely used as drug delivery systems for a variety of drugs. For example, nanoparticle-based drug delivery systems have considerable potential for treatment of tuberculosis (Gelperina *et al.*, 2005). The important technological advantages of nanoparticles used as drug carriers are high stability, high carrier capacity, feasibility of incorporation of both hydrophilic and hydrophobic substances, and

feasibility of variable routes of administration, including oral application and inhalation. Nanoparticles can also be designed to allow controlled and sustained drug release from the matrix. These properties of nanoparticles enable improvement of drug bioavailability and reduction of the dosing frequency, and may resolve the problem of non adherence to prescribed therapy, which is one of the major obstacles in the control of epidemics like that of tuberculosis in developing world tuberculosis (Gelperina *et al.*, 2005).

Using nanoparticles as carriers has emerged as a promising strategy for the efficient delivery of drugs used in the treatment of cancer (Joseph and Sharma, 2008). Nanosponges prepared from β-cyclodextrins as nanoporous materials were found capable of carrying both lipophilic and hydrophilic drugs and of improving the solubility of poorly water-soluble molecules (Cavalli *et al.*, 206). A method to coat functionalized polystyrene spheres with a layer of amorphous titanium dioxide and then turning the so formed core–shell particles into a titanium dioxide nanosponge by calcining the dried particles in a furnace has been described (Guo *et al.*, 208). Recently a nanosponge controlled–release drug delivery system developed at Vanderbilt University was reported to be three to five times more effective than direct injection in that it delayed the *in vivo* tumor tripling time by 55 days (Passarella *et al.*, 2010).

Purpose of the Study

Photodynamic therapy was defined by Henderson and Dougherty (1992) as the combined effect of a photosensitizing drug and light to produce biological damage of therapeutic value, under conditions where neither the light nor the drug operating alone have any effect. The approach has aroused considerable interest in scientific, medical and commercial circles in the last few decades, partly because it is conceptually very exciting, but also because there is no doubt that it works exceptionally well in destroying malignant or otherwise problematic tissue. The basis for photodynamic therapy lies with two remarkable properties of the photosensitizing drugs that are used in the approach – their preferential accumulation in some tissue types notably cancer tissue and the subsequent light triggered toxicity of the photosensitizing drugs used (Henderson and Bellnier, 1989). Photodynamic therapy was initially described as an approach to cancer therapy and Foscan was one of the drugs from Scotia Pharmaceuticals used to treat head and neck cancers (Smeele *et al.*, 2005). In recent times however photodynamic therapy has started to feature in many other health care applications. For instance intravenous injection with Visudyne leads to significant occlusion of the choroidal neovascularization and this has been confirmed by fluoresce in angiography (Kaiser *et al.*, 2009) and used as a basis for the treatment of the wet form of age related macular degeneration. Following the one year VALIO study, the treatment has now been refined and accepted by most clinics in the developed world (Songca and Mbatha, 2000).

Recently a study of the imaging and destruction of cancerous tumours with photodynamic therapy using novel monomeric and dimericporphyrin based photosensitising drug models was developed (Masilela and Songca, 2006). The imaging and photodynamic therapy data using these porphyrins directly and the same porphyrins deposited on magnetic iron oxide-gold core-shell nanoparticles will be collected and compared *in vitro* and *In Vivo*. Two hypotheses will be tested in this planned future work. The first is that porphyrin functionalized iron oxide-gold core-shell nanoparticles will accumulate preferentially in tumor tissue due to the selectivity of the porphyrin for tumor tissue. The second is that the magnetic porphyrin functionalized iron oxide-gold core-shell nanoparticles will be trapped onto a target site, such as a tumour, using a permanent magnet. Furthermore, the magnetic porphyrin functionalized iron oxide-gold core-shell nanoparticles in the tumor tissue can be used to preferentially increase the temperature of the tumor using magnetic hyperthermia. These proofs of concept studies require preparation of magnetic iron oxide-gold core-shell nanoparticles, followed by deposition of the porphyrins on the gold surface. This paper reports on the preparation and characterization of the iron oxide-gold core-shell nanoparticles and the deposition of a porphyrin with four thioacetyl side chains on the gold surface of the particles.

Preparation of the iron oxide-gold core-shell nanoparticles

A number of methods have been developed by various workers for the preparation of superparamagnetic iron oxide nanoparticles (Carvell *et al.*, 2009; Chin and Yaacob, 2007; Guzmán *et al.*, 2008; Kim *et al.*, 2008; Kim *et al.*, 2001; Kinoshita *et al.*, 2003; Maity *et al.*, 2007; Pham *et al.*, 2008; Presa *et al.*, 2007; Oluwafemi and Revaprasadu, 2009) and perhaps the most recent were by Carvell *et al.*, (2009), Guzmán

et al., (2008), Kim *et al.,* (2008) and Maity *et al.,* (2007) All these methods were examined with the aim of preparing iron oxide nanoparticles, combining various aspects from these earlier works to give the methodology of the work reported in this paper.

The gold coating process

The gold coating was accomplished by overgrowing a gold layer onto the iron oxide nanoparticles through the reduction of auchloric acid with sodium citrate in the presence of the as-synthesized iron oxide nanoparticles (Pham *et al.,* 2008). In these reactions, some of the auchloric acid reduction leads to the formation of gold nanoparticles without overgrowing any iron oxide nanoparticles. The desired magnetic iron oxide nanoparticles that are overgrown with gold through this process are thus separated from the non-magnetic gold nanoparticles that have not overgrown any iron oxide nanoparticles, by means of a 3000G permanent magnet (Pham *et al.,* 2008).

MATERIALS AND METHODS

Dichloromethane and triethylamine were distilled from anhydrous calcium hydride. Ferric (III) chloride hexahydrate ($FeCl_3.6H_2O$, >99%), ferrous (II) chloride tetrahydrate ($FeCl_2.4H_2O$, >99%), hydrogen tetrachloroaurate (III) hydrate ($HAuCl_4$), sodium citrate dehydrate ($Na_3C_6H_5O_7.2H_2O$, >99%), ammonium hydroxide (NH_4OH) were obtained from Sigma-Aldrich Logistic, Germany. The other chemicals were of analytical grade from local suppliers and were used without further purifications. All aqueous solutions were prepared using Millipore purified water (18.2 $M.\Omega cm^{-1}$).

Synthesis of the Iron Oxide Nanoparticles

$FeCl_3.6H_2O$ (4.64g, 17 mmol) and $FeCl_2.4H_2O$ (1.71g 8.5 mmol) was dissolved in 250 ml deoxygenated water. To this vigorously stirred and nitrogen atmosphere-protected solution, a mixture of freshly deoxygenated NH_4OH (1M, 100 ml) and $Na_3C_6H_5O_7.2H_2O$ (1M, 19 ml) was added at a rate of 4 ml/min, resulting in a pale yellow color solution changing to brown and finally to dark black. Stirring was continued for an additional 30 minutes at 80-90^oC, and then the solution was cooled to room temperature. This procedure is illustrated schematically in figure 1. The iron oxide nanoparticles so formed were not isolated, but immediately used for the subsequent gold coating process.

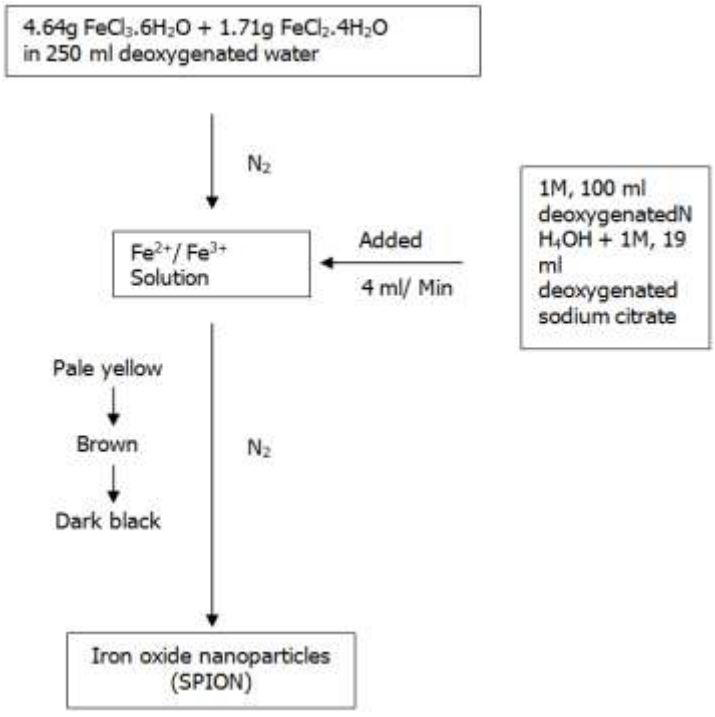

Figure 1: Synthesis of Iron Oxide Nanoparticles

Research Article

Gold Coating of the Iron Oxide Nanoparticles

As-synthesized suspension of iron oxide nanoparticles (1.2ml) was transferred into 200 ml deionized water. After addition of $Na_3C_6H_5O_7.2H_2O$ (155.2 mM, 0.7 ml), this mixture was stirred vigorously and then heated to boil. Once boiling, $HAuCl_4$ solution (10 mM, 10 ml) was injected as quickly as possible, and the initially pale yellow solution changed color to brown, dark brown, and finally to the deep red color characteristic of gold colloids. The heating mantle was removed, and the stirring was continued for an additional 15 minutes as the reaction mixture cooled to ambient temperature. The iron oxide nanoparticles that are gold coated through this process were separated by means of a 3000G permanent magnet, decanting the rest of the suspension containing the gold nanoparticles. This procedure is illustrated schematically in figure 2.

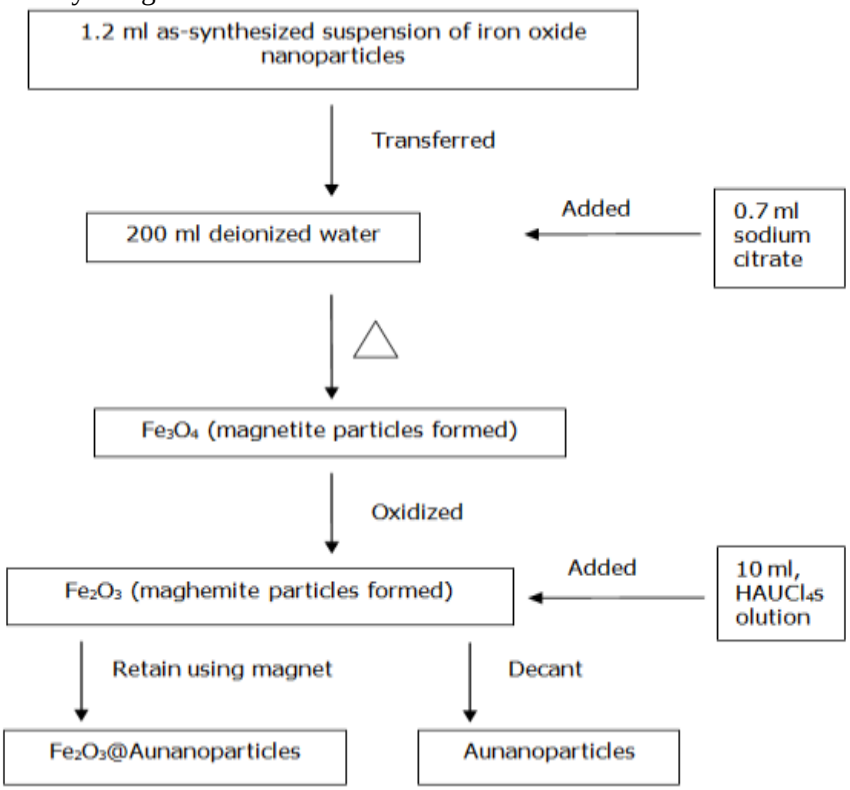

Figure 2: Schematic diagram showing the process for the coating the iron oxide nanoparticles with gold leading to the formation of iron oxide-gold core-shell nanoparticles (Fe_2O_3@Au NPs)

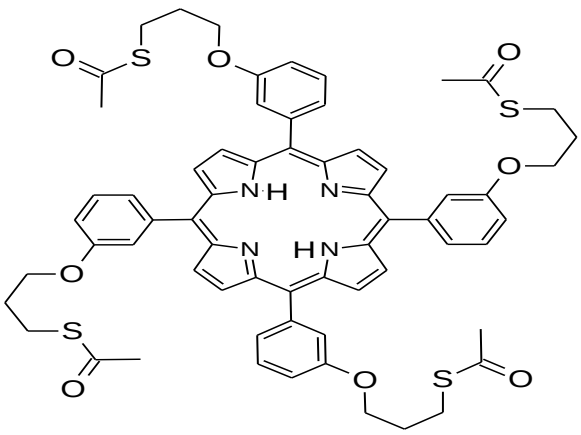

Figure 3: 5,10,15,20-Tetrakis(3-thioacetoxy-1-propyloxy)phenylporphyrin (1).[22]

Deposition of the porphyrin

In this work, the method according to Schweizer *et al.*, was adopted for the synthesis of the thioacetylated porphyrin (1). Theporphyrin was deposited on the gold surface of the iron oxide-gold, core-shell nanoparticles by shaking together equal volumes of a 0.5 mM solution of (1) in chloroform and a 0.5 mM suspension of the iron oxide-gold, core-shell nanoparticles. Upon completion of the phase transfer of the nanoparticles, the bottom layer was collected, dried and concentrated in vaccuo to isolate the porphyrin functionalized iron oxide-gold, core-shell particles. The porphyrin functionalized iron oxide-gold core-shell particles were rinsed with chloroform, centrifuged and isolated to ensure that any non-specifically bonded porphyrins are removed.

To monitor the transfer of the iron oxide-gold core-shell nanoparticles from the aqueous to the organic phase using UV visible spectroscopy, equal volumes of 100 mL each of 0.002 mM of porphyrin in chloroform and a suspension of the iron oxide-gold core-shell nanoparticles were transferred into a 250 mL 2-neck flat bottomed flask mounted on a magnetic stirrer, resulting in an organic porphyrin containing phase below and an aqueous nanoparticle containing phase above. The mixture was stirred vigorously and aliquots of each phase were taken at 600 s intervals for UV-Visible measurement.

RESULTS AND DISCUSSION

The iron oxide nanoparticles so formed were characterized with ultraviolet and visible spectroscopy (UV/Vis), X-ray diffraction (XRD) and transmission electron microscopy (TEM). The iron oxide nanoparticles that were gold coated through this process were also characterized using UV/Vis, XRD, TEM, high resolution transmission electron microscopy (HRTEM) and atomic force microscopy (AFM). The magnetic properties of the iron oxide nanoparticles were investigated using SQUID magnetometry. The particle size distributions of the iron oxide-gold core-shell nanoparticles were measured from the TEM micrographs. The kinetics of the phase transfer reaction of the iron oxide-gold core-shell nanoparticles were investigated using UV/Vis spectrophotometry. The deposition of the porphyrin was investigated with infrared spectroscopy by observing changes in the absorption bands of the thioacetyl groups since the thioacetyl groups are expected to hydrolyse to form the thiol groups through which the porphyrin molecules were expected to enchor on the gold surface of the nanoparticles.

Ultraviolet and Visible Spectroscopy

The UV spectra of the iron oxide nanoparticles (figure 4a), and the iron oxide-gold core-shell nanoparticles (figure 4b) show the characteristic plasmonic peak of the iron oxide nanoparticles at 497nm and the plasmonic peak of the iron oxide-gold core-shell nanoparticles at 532 nm, which is characteristic of gold nanoparticles.

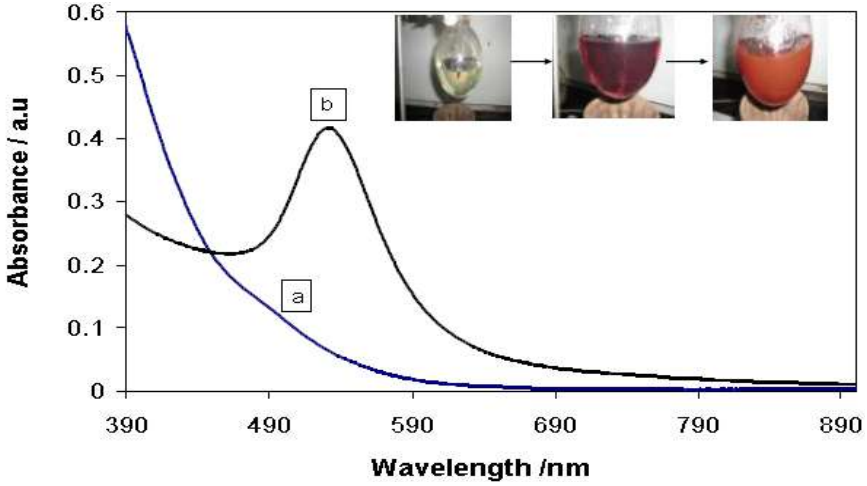

Figure 4: UV spectra of the iron oxide nanoparticles (a), and the iron oxide-gold core-shell nanoparticles (b). (inset: colour of Au-SPION at different stages of synthesis)

Particle Shape and Size Distribution

Typical TEM images of as-synthesized nanoparticles are presented in Figure 5. In general, the particles are spherical in shape and nearly mono-dispersed. The aggregation by some of the particles might be attributed to high surface energy of the bare iron oxide nanoparticles, which enhance adhesion between the nanoparticles of different sizes. It has been proposed that adhesion tends to occur between nanoparticles as a result of dipole-dipole interactions between the highly charged surfaces of the nanocrystals (Oluwafemi and Revaprasadu, 2009; Wang *et al.*, 2006). This adhesion between nanocrystals can induce a significant change on their morphology and hence, cause a transition from dot to elongated particles as a result of oriented attachment or self assembly. Figure 5 shows the fusion between several dot particles, which could lead to the formation of elongated particles.

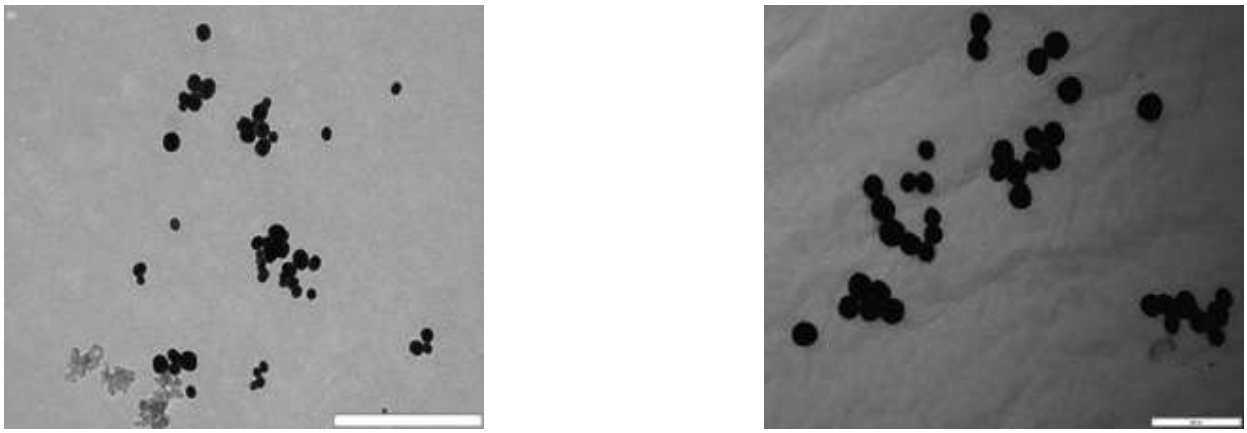

Figure 5: (a) TEM images of iron oxide nanoparticles, (b) iron oxide-gold core-shell nanoparticles

Figure 6 presents histograms of the particle size distribution. The particle sizes for iron oxide nanoparticles (a) are in the range 34–58nm with the mean particle diameter of 42.41 nm ± 12.03 nm and standard deviation (σ) of 0.27 nm indicating broad size distribution. The particle diameters for the iron oxide-gold core-shell nanoparticles (b) are in the range 34–54 nm, with an average particle size as determined from the TEM image of 44.26 nm ± 6.93 nm and standard deviation (σ) of 0.16 nm.

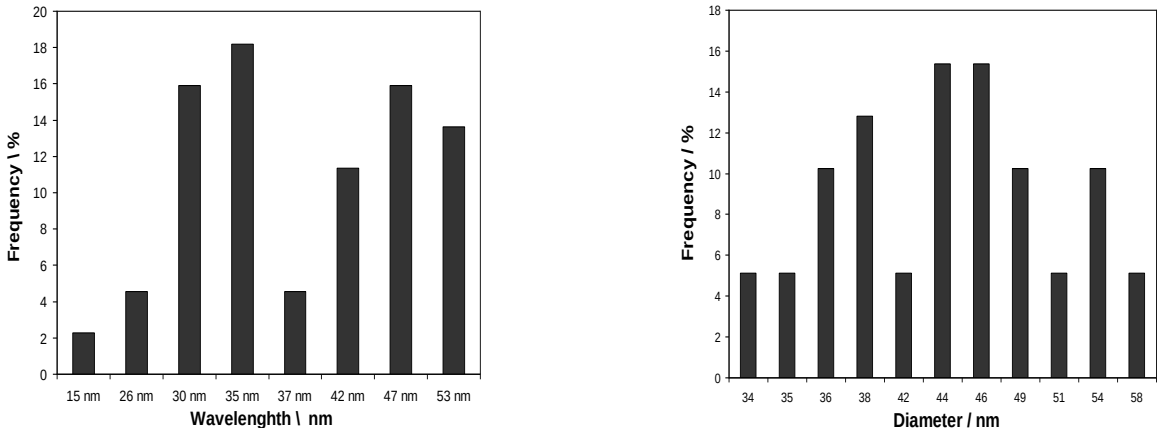

Figure 6: Particle size distribution bars of iron oxide nanoparticles (a), and iron oxide-gold core-shell nanoparticles (b)

Atomic Force Microscopy

The iron oxide-gold core-shell nanoparticles were analyzed with atomic force microscopy (AFM). All the AFM investigations conducted on the sample showed well dispersed nanoparticles on the scanning

surface, thus confirming the results of the TEM examinations. The tapping mode was used and both the height and phase images were captured, using the RTESPW tip at a scan rate of 0.803 Hz. The samples were also scanned with a Platinum Coated tip, SCM-PIT at a scan rate of 1.00 Hz. Typical AFM images using the RTESPW tip and a scan rate of 0.803 Hz, and the platinum coated tip, SCM-PIT at a scan rate of 1.00 Hz are shown in figure 7.

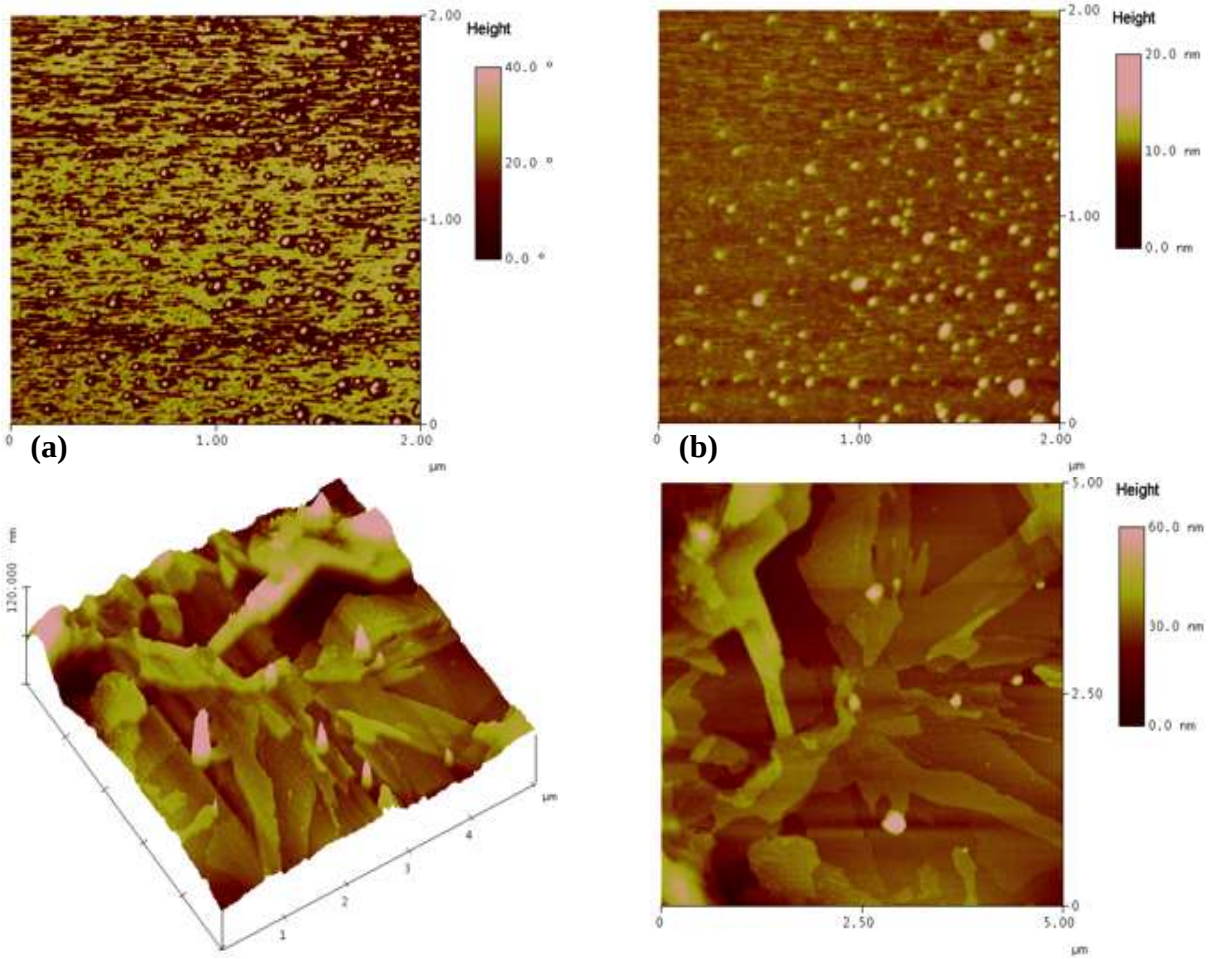

Figure 7: Atomic force microscopy using the RTESPW tip and a scan rate of 0.803 Hz (a), and the platinum coated tip, SCM-PIT at a scan rate of 1.00 Hz (b)

Transmission Electron Microscopy

The iron oxide nanoparticles and the iron oxide-gold core-shell nanoparticles were analyzed with TEM. All the TEM images showed nearly well dispersed iron oxide nanoparticles and iron oxide-gold core-shell nanoparticles. Some images showed evidence of agglomeration and the initial stages of rod formation as nanoparticles came together end-to-end due to inter-particle dipole-dipole attractions as shown in figure 8 (a)–(b) (Oluwafemi and Revaprasadu, 2009; Wang *et al.,* 2006). The high resolution transmission electron micrographs (HRTEM) show the crystallinity of the gold outer shell and that of the iron oxide cores in figure 8 (d).

The HRTEM image (d), shows the existence of lattice planes which confirms the crystallinity of the material. The spacing between adjacent lattice planes is about 0.23 nm which corresponds to the interplanar distance of Fe_3O_4 nanocrystals (Amendola *et al.,* 2011). Figure 8(d) insert is the selected area electron diffraction (SAED) pattern recorded on a single nanoparticle. The SAED patterns are composed of many separated bright spots instead of rings, which imply the single crystal-like diffraction of the

functionalized nanoparticles. The set of brighter spots in the SAED suggests that most nanoparticles have the same orientation. Some disordered spots coexist with ordered bright spots. This phenomenon may be attributed to misarranged nanoparticles (Cheng *et al.,* 2011). The HRTEM and SAED results indicate that most of nanoparticles self-assembled along the same crystal orientation. This phenomenon of oriented aggregation is induced by the spontaneous tendency of nanoparticles to minimize their surface energy (Cheng *et al.,* 2011). Figure 8(c) shows the organic porphyrin layer on the outer surface of the iron oxide-gold core-shell nanoparticles.

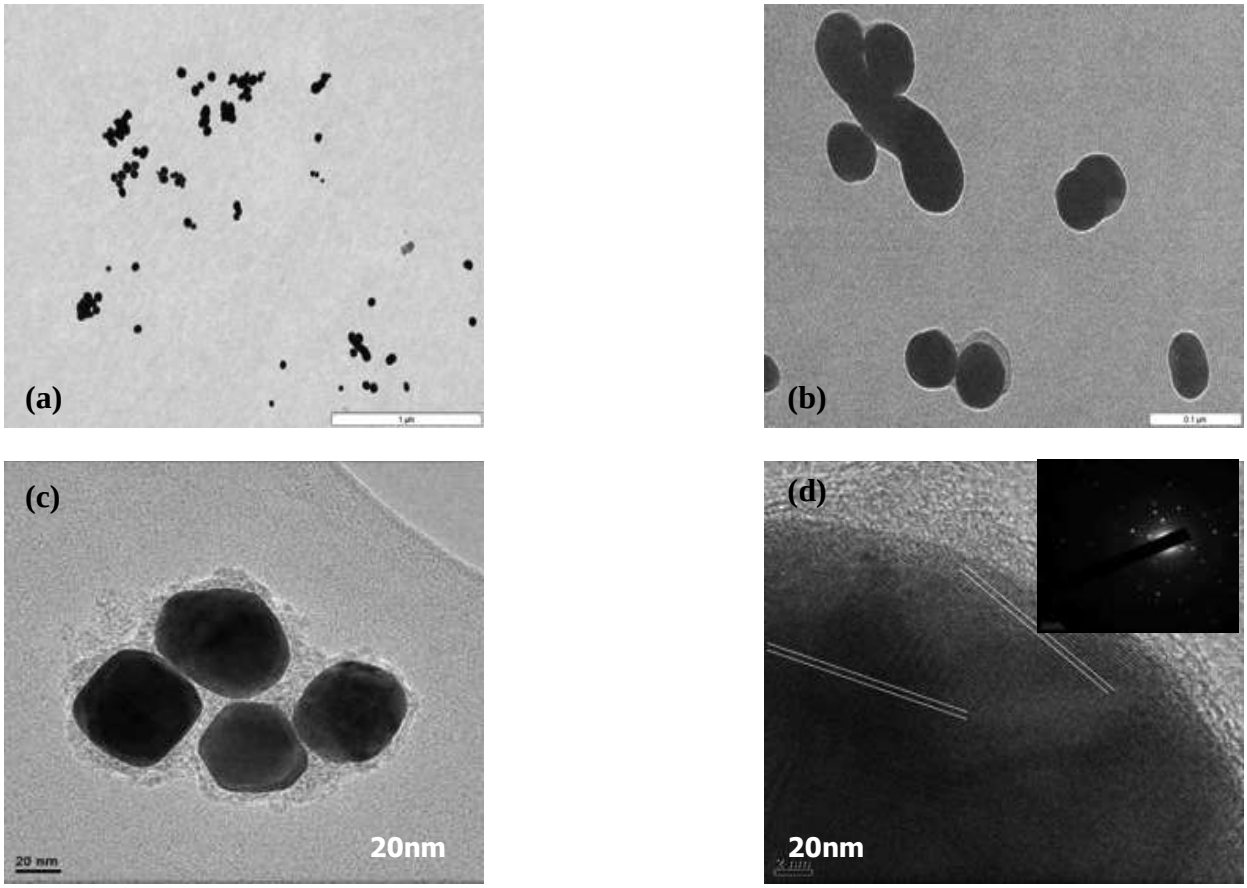

Figure 8: TEM images of iron oxide nanoparticles (a), (b) and iron oxide-gold core-shell nanoparticles (c) HRTEM image of iron oxide-gold core-shell nanoparticles (d)

Infrared Spectroscopy

The deposition of the thioacetoxy-1-propyloxy phenyl porphyrin(1) on the iron oxide-gold core-shell nanoparticles was also studied by comparing the infrared spectrum of the free base porphyrin (figure 9a) with that of the porphyrin functionalized iron oxide–gold core shell nanoparticles (figure 9b). There are two noteworthy observations on the spectrum of the porphyrin functionalized iron oxide–gold core shell nanoparticles. Firstly there is a significant enhancement of the cluster of peaks in the 2950-3200 cm^{-1} region, ascribed to the thiol group bonded to the gold surface of the nanoparticles (Shimazu *et al.*, 1996; Zu *et al.*, 1998). Secondly there is a splitting of the carbonyl stretching frequencies into two peaks. The first observation suggests partial hydrolysis of some of the thioacetyl groups to give thiol groups bonded to the gold surface, while others remain as thioacetyl groups. The second observation suggests that some of the thioacetyl groups may be more closely associated with the gold surface while others remain relatively unassociated.

Research Article

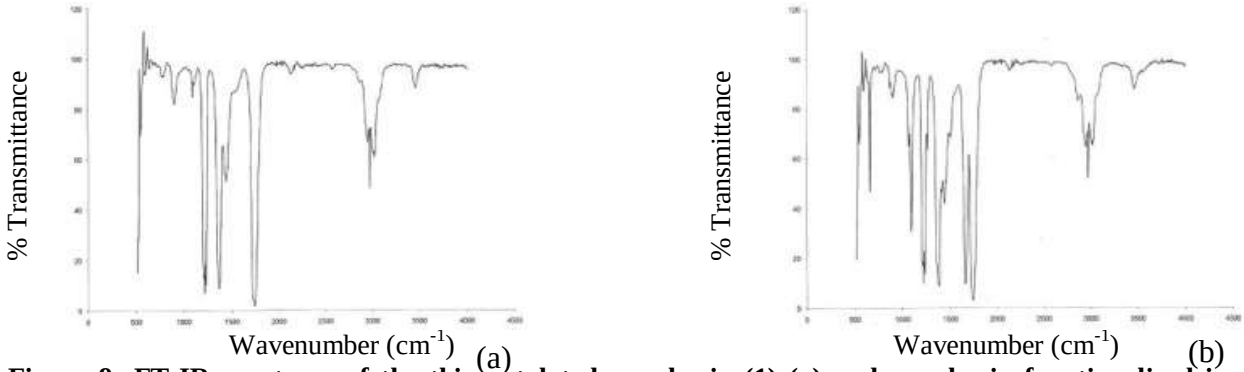

Figure 9: FT-IR spectrum of the thioacetylated porphyrin (1) (a) and porphyrin functionalized iron oxide–gold core shell nanoparticles (b)

Kinetic studies

An indirect procedure was used to measure the rate of adsorbtion of the porphyrin (1) onto the surface of the iron oxide–gold nanoparticles. Monitoring aliquots of the reaction of the aqueous solution based iron oxide-gold core-shell nanoparticles with the porphyrin in the chloroform solution at 532 nm showed that the concentration of the aqueous nanoparticle phase was decreasing over time while the concentration of the organic porphyrin phase was increasing (figure 9), suggesting that the nanoparticles were being transferred from the aqueous phase to the organic phase. In the absence of the dissolved porphyrin, monitoring the aliquots in the same way showed very slow to no such decrease in the absorbance of the aqueous nanoparticle phase and very little to no such increase in the organic phase, indicating that the nanoparticle phase transfer in the presence of dissolved porphyrin in the organic phase was followed by deposition of the porphyrin on the surface of the of the iron oxide-gold core-shell nanoparticles.

Magnetic properties of the iron oxide-gold core-shell nanoparticles

The magnetic properties of a sample of porphyrin functionalised nanoparticles and those of a sample of iron oxide-gold core-shell nanoparticles were studied as function of temperature between 2.0 K and 300 K using a fixed field, as well as two fixed temperatures, viz 2.0 K and 300 K as function of field. For the temperature-dependence studies, both field-cooled and zero-field cooled modes were used. Care was taken to use very small magnetic fields during temperature scans in order to avoid induced or non-spontaneous magnetic effects in the sample. For sample containment, a compressed specimen was held fixed inside a synthetic, magnetically transparent sample holder which has the advantage of being able to avoid spurious signals originating from the glue used as fixing agent. Figure 10(a) shows field-cooled/zero-field cooled (fc/zfc) curves for the porphyrin functionalized, iron oxide-gold core-shell nanoparticles and figure 10(b) shows fc/zfc curves of iron oxide-gold core-shell nanoparticles. The magnetic response of both samples bifurcates between 10 K and 20 K. The implementation of very small fields between 100 Oe and 150 Oe for these measurements lends confidence in determining the spontaneous blocking temperature T_B =15.7 ± 0.1 k and T_B =12.8 ± 0.1 K.

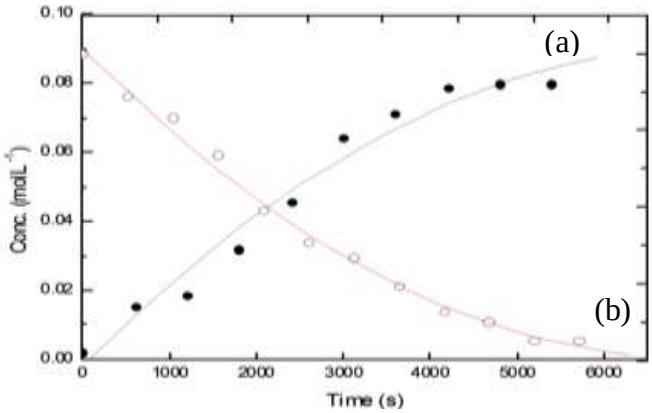

Figure 10: Concentration of nanoparticles in theorganic phase (a) and the aqueous phase (b)

Research Article

Thegraphof field scans at constant temperature in figure 11(a) shows the magnetic response versus field at 300 K for (a) the porphyrin functionalized iron oxide nanoparticles and (b) the iron oxide-gold core-shell nanoparticles. The data collected for increasing magnetic fields were distinguished from that of decreasing fields. There are three notable observations made from the results in figure 11 (1) the magnetic hysteresisis negligible in both cases, as can be seen especially on the magnified scales in the inset of each figure, (2) neither of the two samples could be saturated magnetically, even in applied fields up 25,000 Oe, and (3) the functionalized iron oxide sample reaches a magnetic response of 6.5 times greater than that of the iron oxide-gold core-shell sample at a comparable field of 1,000 Oe.

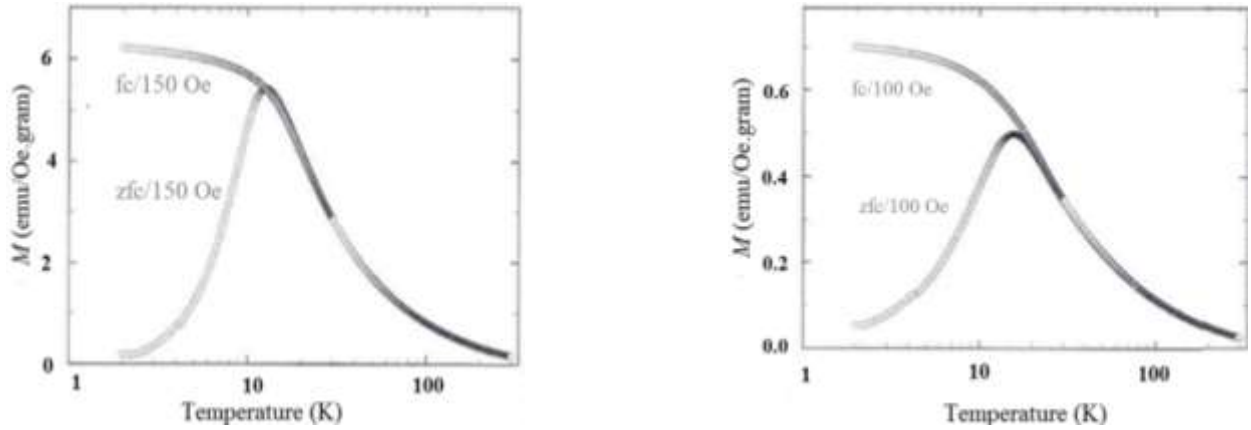

Figure 11: Temperature-dependent magnetic moment of (a) porphyrin functionalized iron oxide nanoparticles and (b) iron oxide-gold core-shell nanoparticles taken in field-cooling and zero-field cooling modes respectively

At all temperatures well below the blocking temperature T_B, a number of observables distinguish the T =2 K< T_B behaviour from that of the high-temperature region. A clear magnetic hystresis is evident at low temperature, as shown in Figure 12. In figure 12 (a), a total hysteresis width of 2,600 Oe is found in the functionalised sample and similarly 2,400 Oe in the case of iron oxide-gold core shell sample.

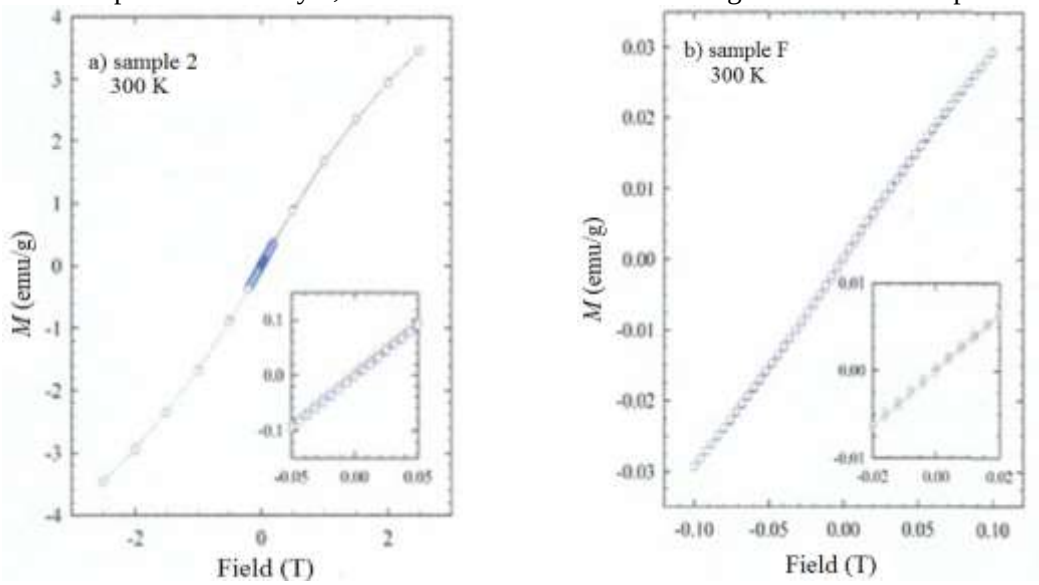

Figure 12: Room-temperature field-dependent measurements of the magnetic moment in (a) porphyrin functionalized iron oxide nanoparticles and (b) iron oxide-gold core-shell nanoparticles. The insets show data near to B=0 in order to emphasize the negligible hysteresis associated with the two samples at room temperature

X-Ray Diffraction Measurements

X-Ray measurements were conducted to investigate the metallic gold and iron content of the iron oxide–gold core shell nanoparticles. The XRD pattern of the iron oxide-gold core-shell nanoparticles is shown in Figure 13. The peaks correspond to the metallic gold diffraction. The pattern of α-Fe is hidden under the pattern of Au due to the overlapping of their diffraction peaks at 2θ = 44.8º, 65.3º, and 82.5º and this confirms the presence of both gold and iron in the sample (Kinoshita *et al.*, 2003).

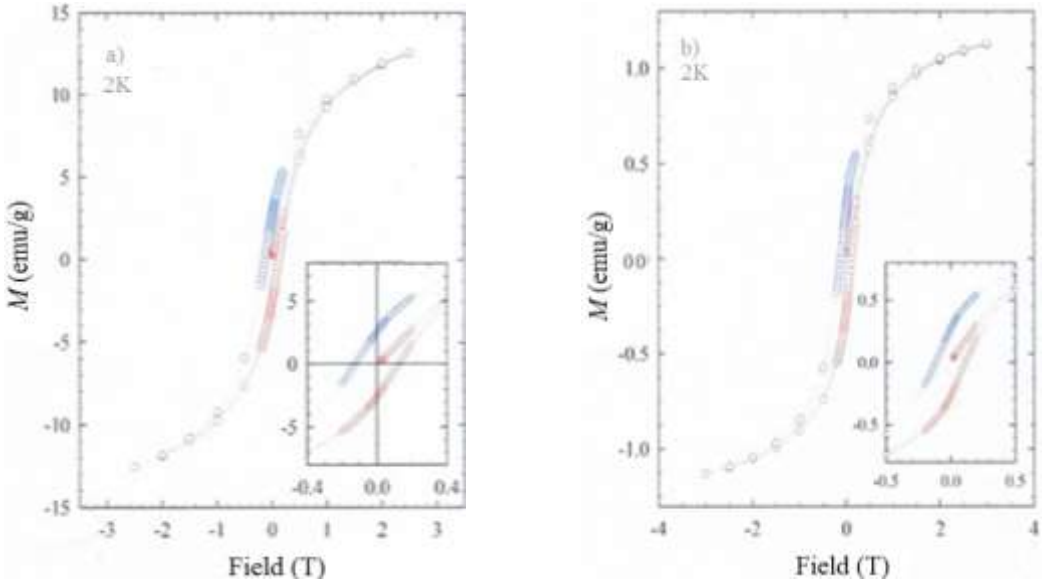

Figure 13: Low-temperature field-dependent measurements of the magnetic moment in (a) porphyrin functionalized iron oxide nanoparticles and (b) iron oxide-gold core-shell nanoparticles. The insets show data near to B=0 in order to emphasize the significant hysteresis associated with the two samples at low temperature, well below the spontaneous blocking temperature

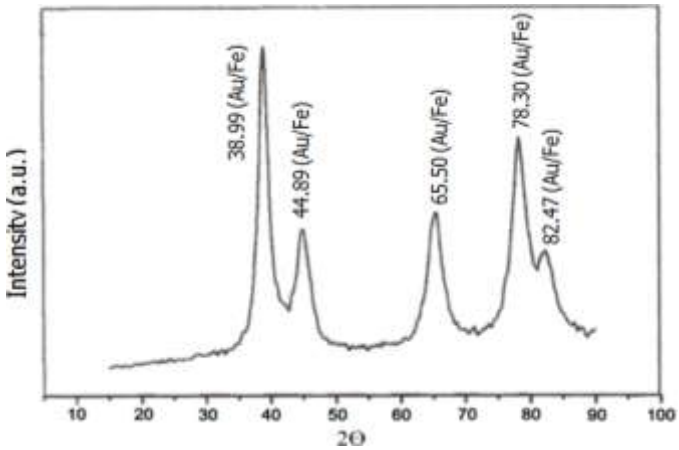

Figure 14: XRD pattern of the iron oxide-gold core-shell nanoparticles

Conclusion

Characterisation of the porphyrin functionalized iron oxide-gold core-shell nanoparticles suggests that they are suitable for the purpose of use as experimental drug delivery systems for photodynamic therapy. Well dispersed iron oxide nanoparticles prepared using the co-precipitation method were successfully overgrown with a gold shell onto the magnetic iron oxide seeds and characterized with TEM, HRTEM, AFM, UV-Vis, XRD and Squid magnetometry. The UV-Vis data confirms that there is an outer shell of

gold and the HRTEM images reveal iron oxide nanoparticles in the interior of the composite nanoparticles. The core-shell structure was thus confirmed by the crystallinity data from the HRTEM images. The particle size distribution data were obtained from the TEM images. The XRD pattern confirms the presence of both iron oxide and gold in the composite nanoparticles. The kinetic studies conducted on the phase transfer reactions of iron oxide-gold core-shell nanoparticles from the aqueous phase to the organic phase suggest that these reactions were followed by deposition of the porphyrin on the surface of the of the iron oxide-gold core-shell nanoparticles once they are in the organic phase. HRTEM images show a layer of porphyrin on the nanoparticles and this is supported by FT-IR data, which shows that some of the thioacetyl groups of the porphyrin have been converted to thiol groups bonded to the gold surface while other remain unbound.

ACKNOWLEDGEMENTS
This work was supported by the NRF Nanoflagships Development Programme. Mintek supported one MSc student and the NRF supported one PhD student. Consumable materials were provided by the University of Limpopo. The authors are grateful for the support of the CSIR for TEM, HRTEM, AFM and XRD data under the MoA between CSIR and WSU and the support of the Physics Department, University of Johannesburg for the SQUID magnetometry.

REFERENCES

Amendola V Meneghetti M Granozzi G Agnoli S Polizzi S Riello P Boscaini A Anselmi C Fracasso G Colombatti M Innocenti C Gatteschi D and Sangregorio C (2011). Top-down synthesis of multifunctional iron oxide nanoparticles for macrophage labelling and manipulation. *Journal of Materials Chemistry* **21** 3803-3813.

Carvell J, Ayieta E, Johnson M and Cheng R (2009). Characterization of Iron Nanoparticles Synthesized by High Pressure Sputtering. *Materials letters* **63**(8) 715-717.

Cavalli R, Trotta F and Tumiatti W (2006). Cyclodextrin-based Nanosponges for Drug Delivery. *Journal of Inclusion Phenomena and Macrocyclic Chemistry* **56** 209-213.

Cheng C, Xu F and Gu H (2011). Facile synthesis and morphology evolution of magnetic iron oxide nanoparticles in different polyol processes. *New Journal of Chemistry* **35** 1072-1079.

Chin AB and Yaacob II (2007). Synthesis and characterization of magnetic iron oxide nanoparticles via w/o microemulsion and Massart's procedure. *Journal of Materials Processing Technology* **191** 235-237.

Gelperina S, Kisich K, Iseman MD and Heifets L (2005). The potential advantages of nanoparticle drug delivery systems in chemotherapy of tuberculosis. *American Journal of Respiratory and Critical Care Medicine* **172** 1487-1490.

Guo L, Gao G, Liu X and Liu F (2008). Preparation and characterization of TiO2 nanosponge. *Materials Chemistry and Physics* **111** 322.

Guzmán MG, Dille J and Godet S (2008). Synthesis of silver nanoparticles by chemical reduction method and their antimicrobrial activity. *Proceedings of World Academy of Science, Engineering and Technology* **33** 2070-3740.

Henderson BW and Bellnier DA (1989). Tissue localization of photosensitizers and the mechanism of photodynamic tissue destruction. In: *Ciba Foundation Symposium 146: Photosensitising Compounds: Their Chemistry and Biological Use* (John Wiley and Sons, Chichester UK) 112-130.

Henderson BW and Dougherty TJ (1992). How does photodynamic therapy work? *Photochemistry and Photobiology* **55** 145-147.

Joseph NM and Sharma PK (2008). Nanoparticle: Drug delivery system for cancer therapy. *Asian Journal of Pharmaceutics* **2** 139-140.

Kaiser PK Registry of the Visudyne AMD therapy writing committee, Boyer DS Garcia R Hao Y Hughes MS Jabbour NM Kaiser PK Mieler W Slakter JS Samuel MTolentino MJ Roth D Sheidow T Strong HA (2009). Verteporfin photodynamic therapy combined with intravitrealbevacizumab for neovascular age related macular degeneration. *Ophthalmology* **116**(4) 747-755

Kim DK, Zhang Y, Voit W, Rao KV and Muhammed M (2001). Synthesis and characterization of surfactant-coated superparamagnetic monodispersed iron oxide nanoparticles. *Journal of Magnetism and Magnetic Materials* **225** 30-36.

Kim KC, Kim EK, Lee JW, Maeng SL and Kim YS (2008). Synthesis and characterization of magnetite nanopowders. *Current Applied Physics* **8** 758-760.

Kinoshita T, Seino S, Okitsu K, Nakayama T, Nakagawa T and Yamamoto TA (2003). Magnetic Evaluation of Nanostructure of Gold-Iron Composite Particles Synthesized by a Reverse Micelle Method. *Journal of Alloys and Compounds* **359**(1-2) 46-50.

Lu QH, Yao KL, Xi D, Liu ZL, Luo XP and Ning Q (2006). Synthesis and characterization of composite nanoparticles comprised of gold shell and magnetic core/cores. *Journal of Magnetism and Magnetic Materials* **301** 44-49.

Maity D and Agrawal DC (2007). Synthesis of iron oxide nanoparticles under oxidizing environment and their stabilization in aqueous and non-aqueous media. *Journal of Magnetism and Magnetic Materials* **308**(1) 46-55.

Masilela I and Songca SP (2006). Synthesis of a porphyrin dimer as a potential photosensitiser in photodynamic therapy. *Journal of Porphyrins and Phthalocyanines* **10** 872.

Oluwafemi OS and Revaprasadu N (2009). Study on Growth Kinetics of Hexadecylamine capped CdSe Nanoparticles using its electronic properties. *Physical B: Condense Matter* **404** 1204-1208.

Passarella RJ, Spratt DE, Van der Ende AE, Phillips JG, Wu H, Sathiyakumar V, Zhou L, Hallahan DE, Harth E and Diaz R(2010). Targeted nanoparticles that deliver a sustained, specific release of Paclitaxel to irradiated tumors. *Cancer Research* **70** 4550-4559.

Pham TTH, Cao C and Sim SJ (2008). Application of citrate stabilized gold-coated ferric oxide composite nanoparticles for biological separations. *Journal of Magnetism and Magnetic Materials* **320** 2049-2055.

Presa P, Multigner M, Morales MP, Rueda T, Fernández-Pinel P and Hernando A(2007). Synthesis and characterization of FePt/Au core-shell nanoparticles. *Journal of Magnetism and Magnetic Materials* 316 e753-e755.

Rosenfeld PJ, Boyer DS, Bressler NM, Fish G, Grizzard WS, Hao Y, Hnik P, Hudson HL, Singerman L and Slakter JS (2007). Verteporfin therapy of subfoveal occult choroidal neovascularization in AMD using delayed light application: one-year results of the VALIO Study. *American Journal of Ophthalmology* **144**(6) 970-972.

Seino S Kinoshita T Otome Y Nakagawa T Okitsu K Mizukoshi Y Nakayama T Sekino T Niihara K and Yamamoto TA (2005). Gamma-ray synthesis of magnetic nanocarrier composed of gold and magnetic iron oxide. *Journal of Magnetism and Magnetic Materials* 293 144-150.

Shimazu K, Takechi M, Fujii H, Suzuki M, Saiki H, Yoshimura T and Uosaki K (1996). Formation and characterization of thiol-derivatized zinc (II) porphyrin monolayers on gold. *Thin Solid Films* **273** 250-253.

Smeele L, Tan B and Copper M (2005). Foscan-mediated photodynamic therapy (PDT) in the treatment of primary squamous cell carcinoma of the head and neck. *International Journal of Oral and Maxillofacial Surgery* **34** 38-38.

Songca SP and Mbatha B (2000). Synthesis of solubilized meso- tetrahydroxyphenylporphyrin photosensitizers by substitution with 2,3-dihydroxy-1-propyloxy groups. *South African Journal of Chemistry* **53** 113-118.

Wang Q, Pan D, Jiang S, Ji X, An L and Jiang B (2006). A solvothermal route to size- and shape-controlled CdSe and CdTe nanocrystals. *Journal of Crystal Growth* **286** 83-90.

Zu R, Ding H, Li W, Wang D and Xi S (1998). FTIR-ATR study of self-assembled thiol monolayers on gold. *Supramolecular Science* **5**(5-6) 607-609.